Sensors & Transducers, Vol. 161, Issue 12, December 2013, pp. 482-492

www.sensorsportal.com

Sensors & Transducers

http.//www.sensorsportal.com

Study on the Vibration Characteristics and Surface Morphology Based on the Surface Hardness Distribution

[1] Songtao Wang, [2] Yongda Yan, [3] Bin Jiang, [4] Minli Zheng,[5] Yihang Fan
[1, 2] School of Mechanical and Electrical Engineering ,Harbin Institute of Technology, Harbin51#, 150066, China
[3, 4, 5] School of Mechanical and Power Engineering, Harbin University of Science and Technology, Harbin, 150080, China

Received: 15 September 2013 /Accepted: 25 October 2013 /Published: 30 November 2013

Abstract: The hardness of hardened steel is one of the key characters of workpiece surface morphology. This paper focus on the instantaneous cutting layer parameters and cutting force under different hardness conditions. Based on the concept of centrifugal force vibration and tool error, the amendatory vibration model of cutting force in milling hardened steels with high speed is established to analyze the influence on the tools vibration characteristics and surface morphology in surface hardness distribution. Through the experiment and simulation, we find the regular pattern that surface hardness distribution influence on vibration and surface morphology. The cutting conditions are also determined for the high-speed milling process, to reach the acquirement of cutting stability and surface morphology on the surface of hardened steel. *Copyright © 2013 IFSA.*

Keywords: Hardened steel, Surface morphology, Vibration.

1. Introduction

The machined surface roughness is used to evaluate the surface quality of products as the requirement of precision machining parts necessary technology. At present, various research works has been carried out on the influence from cutting parameters, tool parameters, processing conditions on the surface roughness and surface morphology. In the process of milling hardened steel with high speed, the vibration is controlled by the tool, workpiece hardness, cutting parameters and other factors. It is necessary to study the regular pattern of vibration characteristics' influence on the surface morphology to ensure that effect of stability of the machining process, surface quality, machining accuracy and so on.

C. R. Liu from Purdue University found that lower Impact tool wear brings lower wear on residual stress [1]. C.R. Liu modeled, emulated and optimized the residual stress on the machined surface of the hardened steel [2]. A. M. Abrao and D. K. Aspinwall [3] tried mechanical engineering and manufacturing respectively ceramic used CNC or PCBN tools to cut steel AISIE52100, to find the existence of residual compressive stress in the surface of the workpiece. D. W. Wu and Y. Matsumoto found that the hardness of the workpiece affects the surface integrity greatly and positively [4]. D. A. Axinte focused on the high speed milling process of hardened steel (HRC51-53) surface integrity, and found that the machined surface residual stress decreases with the increase of cutting speed and feed per tooth, but the residual stress of surface roughness can't reach the best value [5]. X. L.

Article number P_RP_0030

Liu found that cutting speed, feed rate and cutting depth have a single variation on surface hardness [6]. The white layer is another important factor affecting the cutting quality of the machined surface, and it is accompanied by an organization formed in hard cutting process. Y. K. Chou and C. J. Evans analyzed the formation of white layer during hard cutting process and found that the tool flank wear will lead to the increase of the depth of white layer [7]. B. J. Griffiths also found that the white layer's relation with the product and tool wear mainly [8].

The hardness of the workpiece has a significant effect on cutting force and tool wear [9, 10]. In the milling and hardness splicing work, the hardness change of the tool and workpiece contact zone increase tool wear, reduce the processing surface quality and restrict the produce efficiency. Milling vibration law is very complex. Analyze time domain and frequency spectrum of the acceleration signal is an effective means to study the cutting vibration. Tatar studied the harmonic characteristics of vibration signals [11]. Using the power spectral density function, Amina analyzed the relationship between the surface roughness of steel milling and vibration amplitude [12]. Toh analyzed the difference of the milling force spectrum between the old and new tool, as well as the difference of the milling paths [13]. Liu established a milling vibration test systems [14].

In this paper, variations of cutting vibration during the high speed milling machining for free-form surface hardened steel hardness quenching are analyzed, to find the hardness distribution of machined surface topography, to support quality evaluation of the high speed milling of hardened steel machined surface.

2. High Speed Milling Vibration Model

2.1. Cutting Force Model

In Fig.1 to 3, a geometric model of the instantaneous cutting layer parameters and cutting infinitesimal is introduced.

As a function of the angel of the tool cutting the tentacles θ, the instantaneous floor area of the single tooth cutting tool is written as

$$A_D(\theta)=\int_{z_1}^{z_2}\frac{h_D\cdot R\cdot dz}{\sqrt{R^2-z^2}}+\int_{z_2}^{z_3}\frac{h_D\cdot R\cdot dz}{\sqrt{R^2-z^2}} \qquad (1)$$

The average instantaneous cutting thickness is

$$h_{aV}(\theta)=\frac{1}{\phi_3-\phi_1}\int_{\phi_1}^{\phi_3}\mathrm{h_D}(\phi)\,\mathrm{d}\phi. \qquad (2)$$

The unit cutting force through experiments is

$$p_c(\theta)=\frac{p_{c1.1}}{h_{aV}^u(\theta)}=\frac{(\mathrm{p_{0c1.1}}+\mathrm{k}\cdot\Delta\mathrm{HRC})}{h_{aV}^u(\theta)}, \qquad (3)$$
$$p_{oc1.1}=27521.42\cdot n^{-0.21477},$$

where $p_{c1.1}$ is the cutting force per unit area, and u is the index of h_{aV}'s influence on cutting force per unit area.

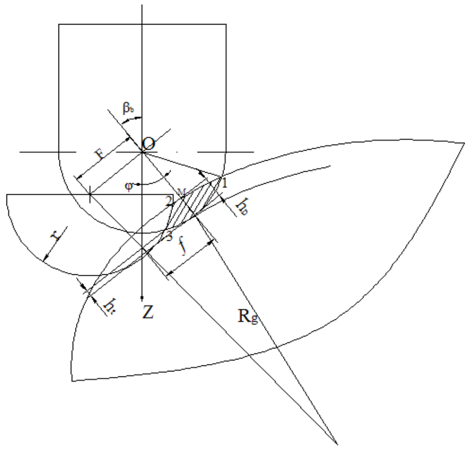

Fig. 1. Instantaneous cutting layer parameters.

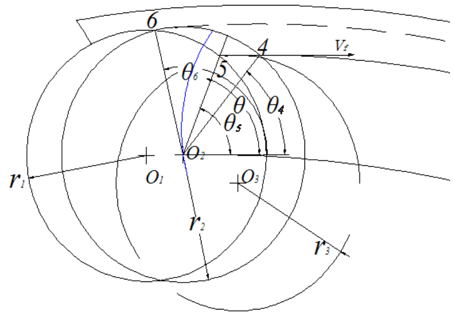

Fig. 2. Cutting layer in top view port.

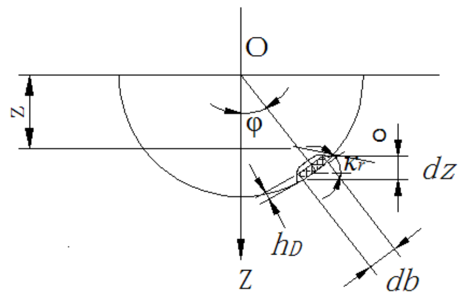

Fig. 3. Cutting micro-elements of ball end mill.

When HRC < 50 k is 93.75 and k is 107.14 when HRC ≥ 50. Considering the action under the speed and hardness, the instantaneous cutting force of ball head end mill is

$$F_c(\theta) = A_D(\theta) \cdot \frac{\left(27521.42 \cdot n^{-0.21477} + k \cdot \Delta HRC\right)}{h_{aV}^{u}(\theta)}, \quad (4)$$

where k is the influence coefficient of workpiece hardness .

2.2. Vibration Model of Cutting Force

In high-speed milling machining process, the centrifugal force of the dynamic cutting forces and tool offset centroid is the main forced excitation of the tool vibration. Under the action of centrifugal force and the dynamic cutting, the tool will relatively slight make displacement or rotation to save energy, which exhibits both elastic and damping characteristics.

Because the stiffness of the z direction is much larger than the other directions, the tool and the workpiece in contact in a plane perpendicular to both the two degree of elastic-damping freedom system with the basic physical model of high-speed milling dynamics,

$$\begin{aligned} F_x^{'}(t) &= m_x x^{''}(t) + c_x x^{'}(t) + k_x x(t) \\ F_y^{'}(t) &= m_y y^{''}(t) + c_y y^{'}(t) + k_y y(t), \end{aligned} \quad (4)$$

where $x(t), y(t), x^{'}(t), y^{'}(t), x^{''}(t), y^{''}(t)$ are the vibration displacement, velocity and acceleration in X, Y direction of the machine tools respectively. m_x, m_y , c_x , c_y , k_x and k_y are the model mass, damping and stiffness in X, Y direction of the tools respectively.

Excitation caused by cutting force can be expressed as

$$F_c = K_c^{'} \cdot A_c + \tan\gamma_0 \cdot K_r^{'} \cdot A_c \quad (5)$$

$$F_r = K_r^{'} \cdot A_c - \tan\gamma_0 \cdot K_c^{'} \cdot A_c \quad (6)$$

$$K_c^{'} = K_c (f_z \sin\phi)^{-m}, \quad (7)$$

$$K_c^{'} = K_c (f_z \sin\phi)^{-m}, \quad (8)$$

where A_c is the cutting area, f_z is the feed engagement per tooth (mm/z), k_r is the milling cutter main deflection angle (°), k_c is the tangential cutting force units, k_r is the axial cutting force units, m is the experience index (m=0.210).

According to the superposition principle of cutting force, we have

$$F_x = F_{rtotal} \sin\phi - F_{ctotal} \cos\phi \quad (9)$$

$$F_y = F_{ctotal} \sin\phi - F_{rtotal} \cos\phi, \quad (10)$$

where F_{rtotal} is the sum of F_r, F_{ctotal} is the sum of F_c, and ϕ is the angel of the feeding direction (°).

2.3 Deflection Model of Centrifugal Force

Centrifugal force F_e is caused by the imbalance incentive tool:

$$F_e = me(2\pi n / 60)^2, \quad (11)$$

where m is the milling mass, e is the milling quality eccentricity.

In the high speed milling process, the vibration value of the tool tip is superimposed by the entire spindle after vibration cutter and cutter system. In the course of spindle rotation, elastic and plastic deformation of the tool system, the offset of the spindle, the elastic deformation of the machine tool will be superimposed on the tool. Because equation (12) is for centrifugal machine tool in the ideal state, the actual tool vibration offset $S^{'}$ to S . So the amendment deflection model of centrifugal force is

$$F_e = me^{'}(2\pi n / 60)^2, \quad (12)$$

where $e^{'}$ is the equivalent eccentricity of the tool.

Because $e^{'}$ is influenced by the tool system, machine spindle and performance factors of the bed and so on, it is complicate to solve the problem. It can be measured by an experiment which the machine idle away. Each machine matching the corresponding $e^{'}$ makes the model more accurate. Idling in high speed, tool systems are affected by initial centrifugal force. The initial displacement leads to the migration of the mass center of tool, thereby generates new eccentricity $x(t)$ and centrifugal force F_e. So after infinite superposition, the physical model should be like the one in Fig.1 when it establishes the balance. S is the maximum amplitude value of the idling centrifugal force excitation, $S^{'}$ is the actual offset of the tool deflection, $S^{''}$ is the offset of the tool system and machine bed.

In the superposition process of two kinds of excitation, a single-excitation vibration model is analyzed first. Then new vibration model for two different excitations is superimposed. The centrifugal and cutting force should not be superimposed in the first step, because they may lead to change of the superposition excitation frequency, and to reduce the vibration analysis accuracy. In the vibration superposition model, the maximum deflection of the tool $S^{'}$ should be split into S_x and S_y firstly, as a function of the phase angle of the unbalanced center of the tool mass φ,

$$S_x = S\sin(2\pi nt/60+\varphi) \tag{13}$$
$$S_y = S\cos(2\pi nt/60+\varphi). \tag{14}$$

2.4 Model of Tool Error

In the cutting process, there are natural phenomena of deflection in the tool tip position because the tool may not reach the absolute symmetry in the manufacturing process. At the same time, there are installation errors from tool and cutter blade in the installation process. Because of the tool wear, there are differences between ideal and reality in the geometry and position of the tool. The error of cutter W is introduced to express the offset between the ideal and actual position, and W is split into (W_x, W_y),

$$W_x = W\sin(2\pi nt/60+\varphi) \tag{15}$$
$$W_y = W\cos(2\pi nt/60+\varphi) \tag{16}$$

In cutting process, the locating datum is not coincident with the design reference because of tool errors. It affects the accuracy and applicability of the theory model. In this paper, only the error of cutter blade caused by installation accuracy is considered.

2.5 Amendment Vibration Model

After (W_x, W_y, S_x, S_y) and $(F_x^{'}, F_y^{'}, F_x, F_y)$ are substituted in the equation (5), we have

$$x(t) = \frac{F_x{'} - m_x x''(t) - c_x x'(t)}{k_x} \tag{17}$$

The total tool vibration is

$$x_{total}(t) = W_x + S_x + \frac{F_x{'} - m_x x''(t) - c_x x'(t)}{k_x} \tag{18}$$
$$y_{total}(t) = W_y + S_y + \frac{F_y{'} - m_y y''(t) - c_y y'(t)}{k_y}. \tag{19}$$

3. Experiments on the Machined Surface Morphology

3.1. Experimental Conditions

In the following experiments, Cr12MoV and 7SiMnMoV are used as materials, and MIKRON UCP710 Five axis CNC milling machining center is the machine tool, and carbide end mill (diameter 20 mm, 4 blades, Spiral Angle 45°, and overall length 92 mm) is the cutting tool. The other cutting parameters are shown in Table 1.

Table 1. Experimental parameters.

No.	*n* (r/min)	f_z (mm/z)	a_e (mm)	λ (°)	a_p (mm)
1-1	5000	0.3	0.3	15	0.2
1-2	6000	0.3	0.3	15	0.2
1-3	7000	0.3	0.3	15	0.2
1-4	8000	0.3	0.3	15	0.2

To get experimental data including the surface hardness, cutting force, cutting temperature, cutting vibration, surface roughness and so on, the equipment used in experiment are shown in Fig. 4, including Kistler 9257B dynamometer, ThermoVision A40M thermal infrared imager, SD1403 acceleration sensor, TR200 surface roughness tester and VHX-600 optical microscope.

Fig.4. Test equipment in experiment.

The test points of the specimen surface are shown in Fig. 5.

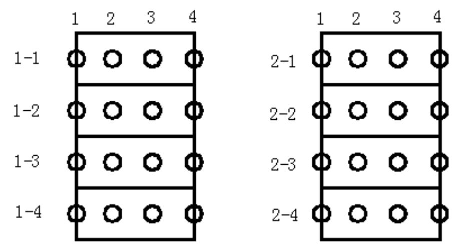

a) Cr12MoV b) 7SiMnMoV

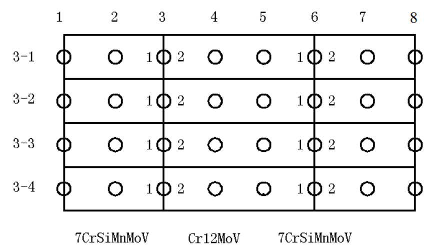

c) Splice specimens

Fig. 5 . Test points diagram of hardness and surface roughness.

3.2. Test of the Surface Hardness

The surface hardnesses in test are shown in Tables 2-4.

Table 2. Hardness of hardened steel workpiece (Cr12MoV).

1	HRC			
	1	2	3	4
1-1	46.8	54.0	55.1	50.5
1-2	55.4	54.3	56.7	56.7
1-3	57.7	56.8	56.7	57.1
1-4	57.8	57.5	57.5	57.0

Table 3. Hardness of hardened steel workpiece (7SiMnMoV).

2	HRC			
	1	2	3	4
2-1	17.3	18.7	18.9	18.4
2-2	16.6	16.9	18.2	18.7
2-3	13.3	16.8	18.1	17.7
2-4	14.7	15.9	16.8	16.6

3.3. Machined Surface Morphology and Roughness of the Hardened Steels

The test results of Cr12MoV and 7CrSiMnMoV splicing piece surface are shown in Table 5. The micro morphology of each point are shown in Fig. 6-11.

Table 4. Hardness of splicing workpiece.

	7SiMnMoV (HRC)			Cr12MoV(HRC)				7SiMnMoV(HRC)		
	1	2	31	32	4	5	61	62	7	8
3-1	25.0	17.2	24.4	54.7	52.4	55.7	54.9	12.7	13.6	15.7
3-2	22.7	21.5	21.3	55.8	56.4	56.7	56.4	15.2	15.9	14.7
3-3	21.8	22.7	21.9	56.8	56.6	57.3	57.0	13.6	15.2	15.4
3-4	22.6	22.5	23.7	55.5	56.4	56.4	57.0	14.1	15.7	16.8

Table 5. Surface roughness results of splicing workpiece.

	R_a (μm)									
	1		2		3		32		4	
	Row	Feed	Row	Feed	Row	Feed	Row	Feed	Row	Feed
3-1	0.490	0.386	0.451	0.350	0.430	0.359	0.382	0.318	0.353	0.387
3-2	0.449	0.449	0.461	0.479	0.461	0.443	0.435	0.180	0.379	0.190
3-3	0.623	0.752	0.773	1.078	0.800	0.929	0.751	0.812	0.726	0.834
3-4	0.497	0.565	0.450	0.460	0.700	0.407	0.200	0.246	0.226	0.138
2	5		61		62		7		8	
	Row	Feed	Row	Feed	Row	Feed	Row	Feed	Row	Feed
3-1	0.337	0.344	0.385	0.356	0.556	0.369	0.398	0.353	0.461	0.288
3-2	0.286	0.277	0.272	0.225	0.602	0.365	0.481	0.332	0.430	0.434
3-3	0.793	0.867	0.426	0.860	0.942	0.419	0.822	0.866	0.861	0.781
3-4	0.160	0.162	0.180	0.150	0.313	0.300	0.307	0.362	0.375	0.410

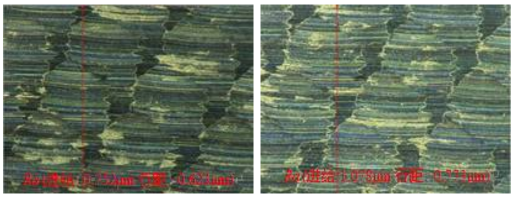

a) 3-3-1 b) 3-3-2

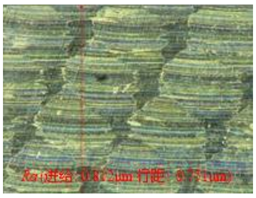

c) 3-3-3

Fig. 6. Surface morphology when cutting into splicing workpiece (material. 7SiMnMoV).

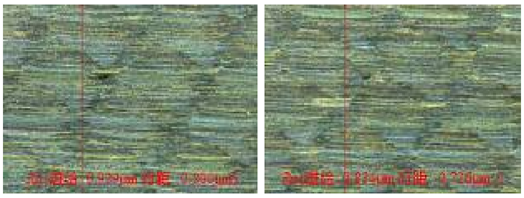

a) 3-3-3 b) 3-3-4

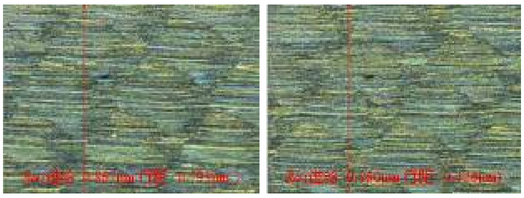

c) 3-3-5 d) 3-3-6

Fig. 8. Surface morphology of the middle part of splicing workpiece (material. Cr12MoV).

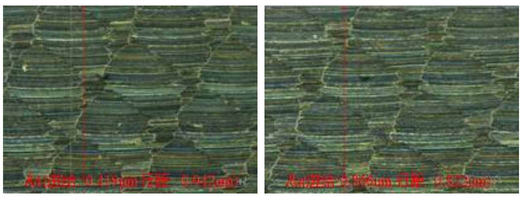

a) 3-3-6 b) 3-3-7

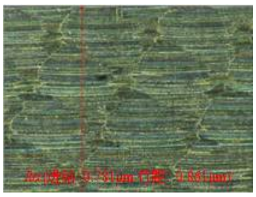

c) 3-3-8

Fig. 10. Surface morphology when cutting out splicing workpiece (material 7SiMnMoV).

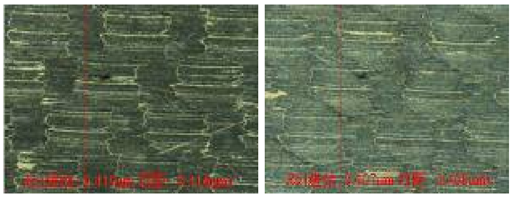

a) 2-3-1 b) 2-3-2

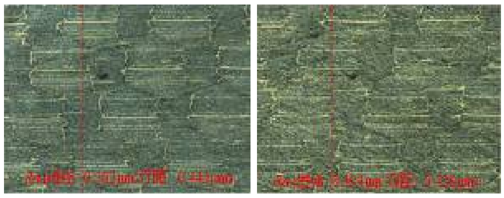

c) 2-3-3 d) 2-3-4

Fig. 7. Surface morphology of 7SiMnMoV when machining single workpiece.

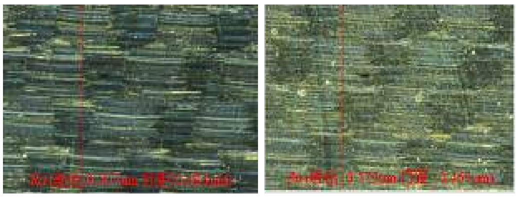

a) 1-3-1 b) 1-3- 2

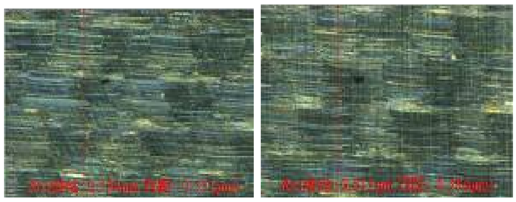

c) 1-3-3 d) 1-3-4

Fig. 9. Surface morphology of Cr12MoV when machining single workpiece.

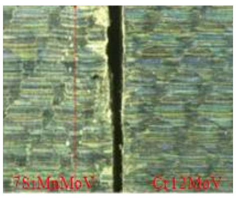

a) 7CrSiMnMoV and Cr12MoV

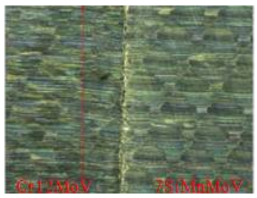

b) Cr12MoV and 7CrSiMnMoV.

Fig. 11. Comparison of surface morphology of splicing part.

Table 6. The simulation results of hardness distribution and vibration amplitude.

Speed r/min		1		2		3		4	
		Hardness	Amplitude	Hardness	Amplitude	Hardness	Amplitude	Hardness	Amplitude
3000	feed row	46.8	31.5 28.5	54.0	35 31.5	55.1	35.5 32	50.5	33.75 30.25
4500	feed row	55.4	35.2 30.25	54.3	34.75 30.25	56.7	35.5 30.75	56.7	35.5 30.75
6000	feed row	57.7	35.25 31.5	56.8	34.9 31.15	56.7	34.9 31.15	57.1	35.09 31.6
8000	feed row	57.8	37.5 32.63	57.5	37.35 32.5	57.5	37.35 32.5	57.0	37 31.5

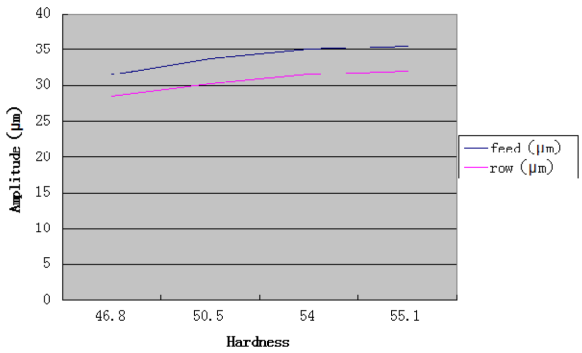

(a) 3000 turn.

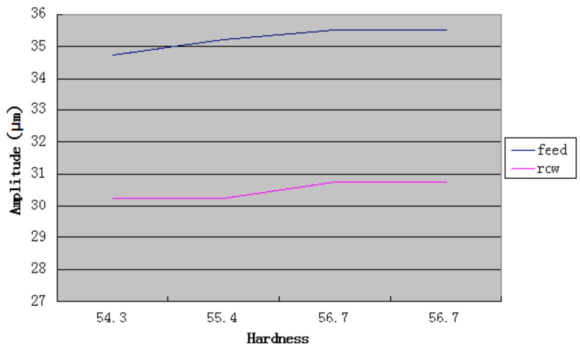

(b) 4500 turn.

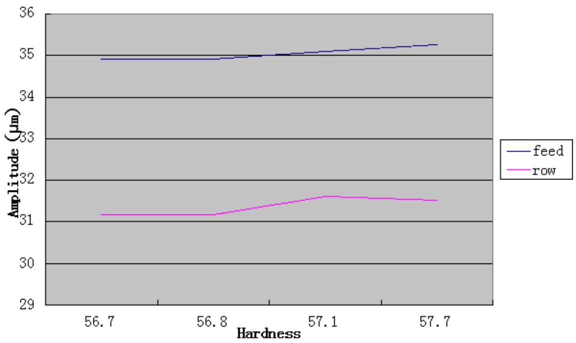

(c) 3000 turn.

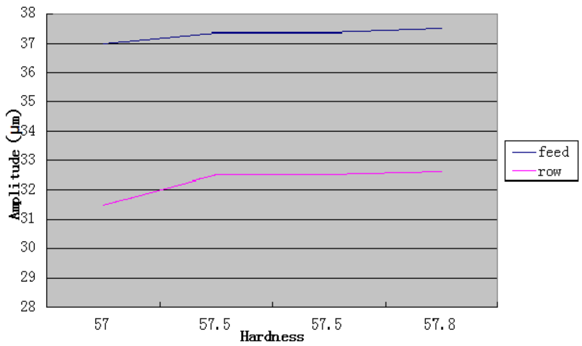

(d) 8000 turn.

Fig. 12 The hardness of the workpiece's impact on cutting vibration.

3.4. Effect of Hardness Distribution on the Cutting Vibration

According to the experimental parameters and hardness distribution, simulation of cutting vibration, Cr12MoV hardened steel hardness distribution and vibration amplitude component are shown in Table 6.

From the table, one conclusion can be drawn that the hardness of the workpiece has a position effect on cutting vibration amplitude at all different speeds, and the trend diagrams are shown in Fig. 12. At different speed, the amplitudes of the feed direction are higher than those of the row direction. When the hardness increase, the row direction vibration increases, and the surface roughness increase in milling direction at the same time. The feeding direction vibration increases when surface roughness decreases. The hardness affects the surface roughness through the cutting vibration.

3.5. Influence of Hardness Distribution on Surface Morphology

Cutting splicing die when spindle speed reaches 6000 rpm, then the surface morphology and surface roughness is analyzed. The test points of the surface morphology and surface roughness is 1mm away from the workpiece edge. When the tool has just entered the 7SiMnMoV specimens (Fig. 6), the workpiece punched the tool. But there was no significant difference from the surface roughness value, which indicated that the hardness of the workpiece surface had no effect on the edge of workpiece surface when the tool gets into it. The surface roughness increases significantly after the tool cut out, indicating that the hardness of the workpiece surface makes the surface quality of the workpiece edge worse respectively. During the cutting of 7SiMnMoV separately, the surface roughness value of the edge is in comparison with other location (Fig. 7), the surface roughness in the milling direction is 0.528 μm, which is evidently higher than the value in the feeding direction, 0.394 μm as the average level.

When the tool is cutting off 7SiMnMoV and is cutting into hardened steel Cr12MoV at the same time (Fig. 8), the sudden increase of hardness impacts the tool, but the surfaces roughness has no obvious change. When cutting out the hardened steel Cr12MoV specimens (Fig. 9), the roughness value of the surface increase, which indicates that the dynamic cutting force of the tool is not completely disappeared when the hardness jumps. Comparing the hardened steel Cr12MoV specimen in the splicing piece with the hardened steel Cr12MoV, the surface roughness of cutting the specimen separately is 0.5-0.6 μm, in the splicing piece is 0.7-0.9 μm. The surface roughness of the workpiece of high hardness near the starting point is inconspicuous difference with other parts, which make the roughness of the workpiece of surface hardness raise in the range of sizes of experimental works. Direct cutting brings a powerful impact on the tool because the hardness of the specimen of Cr12MoV hardened steel is very high. In order to mitigate this impact, it is better to cut the splicing workpiece from low hardness area to high hardness area.

When the tool is cutting off the Cr12MoV hardened steel and is cutting into 7SiMnMoV at the same time (Fig. 10), the hardness of the workpiece becomes low suddenly. In the feeding direction the surface roughness is 0.419 μm, which is significantly lower than other parts. In the milling direction the surface roughness is 0.942 μm, which is significantly higher. The surface roughness at the edge of the workpiece has no obvious change (Fig. 7), which indicate that the violent vibration of cutting the Cr12MoV hardened steel specimens still exists at this time, and the surface roughness at the edge of the 7SiMnMoV is significant different with other parts. The surface roughness for 7SiMnMoV specimen is 0.4-0.8 μm, and in the splicing workpiece is 0.3-0.5 μm. So cutting the surface of the workpiece surface from high hardness to low hardness is in favor of the control of the roughness degree.

In summary, in order to ensure the surface quality of different hardness splicing piece, the cutting process should be start from low hardness parts, and cut off from the low hardness.

To the surface roughness and surface hardness of the splicing die, the hardness of Cr12MoV hardened steel specimen is HRC50-60, and of the 7SiMnMoV specimen is HRC15-25, so there is obvious tremendous difference. The surface roughness of the workpiece of Cr12MoV hardened steel is lower than 7SiMnMoV specimen's in both the milling direction and feeding direction. The reason may be that the hardness of the Cr12MoV hardened steel specimen is very high. It meets the adiabatic shear theory, and there are a few phosphorus thorns in the machined surface. The surface of the 7SiMnMoV test piece is relatively soft without quenching treatment. It also meets the theory of shear slips, producing phosphorus thorn easily in the cutting process and making the surface roughness of the workpiece increase greatly. Fig. 11 shows the surface textures of the two kinds of workpiece splicing site. The surface morphologies are quite different. The micro unit of the Cr12MoV hardened steel machined surface is neat and orderly, but the micro unit of the 7SiMnMoV machined surface is neither clear nor neat. Because the specimen of Cr12MoV hardened steel is a quenched workpiece, it has high hardness and its cutting deformation is low. The hardness of the 7SiMnMoV specimen is relatively lower for no quenching treatment, cutting deformation, built-up edge, phosphorus thorn make the surface morphology angulation.

Generally the surface roughness of the 7SiMnMoV specimen is higher than that of Cr12MoV hardened steel specimen. The surface roughness rises with the raise of the spindle speed, until the spindle speed reaches 8000 rpm, the surface roughness decreases.

3.6. Stable Cutting Conditions on the Surface of Hardness Splicing Workpiece

Hardened steel hardness splicing specimen and experimental fields are shown in Fig. 13.

Spindle speed is 8000 rpm, feed rate is 4000 mm/min, row spacing is 0.3 mm, and the cutting depth is 0.2 mm.

The experimental results of vibration are shown in Table 7.

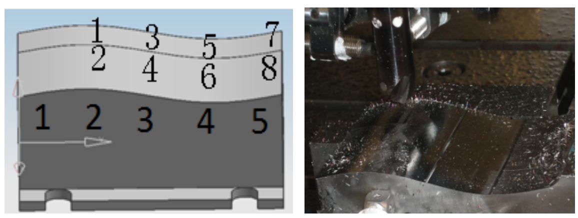

Fig. 13. Splicing workpiece.

Table 7. Experimental results of the vibration in high-speed milling splicing workpiece of Cr12MoV and 7CrSiMnMoV.

No.		Spindle feed amplitude (m/s^2)	Spindle axial amplitude (m/s^2)	Spindle pitch amplitude (m/s^2)	Cutter spacing amplitude (μm)	Cutter spacing spectrum (Hz)	Tool feed amplitude (μm)	The cutter feeding frequency spectrum (Hz)
Parallel to the X axis	1 soft	3.3	2.0	1.6	17.4	134.3	12.3	134.3
	2 hard	3.3	2.0	2.1	18.2	134.3	15.8	134.3
	3 soft	3.5	3.3	1.6	17.2	134.3	12.0	134.3
	4 hard	3.5	2.05	2.1	18.1	134.3	14.55	134.3
	5 soft	3.3	2.2	1.5	17.3	134.3	12.25	134.3
	6 hard	3.6	2.1	2.1	18.2	134.3	14.5	134.3
	7 soft	3.4	2.1	1.6	17.4	134.3	12.35	134.3
	8 hard	3.5	2.0	2.0	18.2	134.3	15.0	134.3
Y shaft angle of 45°	1 soft	3.2	2.0	1.65	15.6	134.3	15.8	134.3
	2 hard	3.5	2.45	1.8	20	134.3	16.2	134.3
	3 soft	3.25	2.05	1.55	16.5	134.3	15.2	134.3
	4 hard	3.3	2.5	1.9	19.6	134.3	16.0	134.3
Parallel to the Y axis	1 soft	2.4	2.0	1.8	17.3	134.3	18.6	134.4
	2 hard	2.0	1.8	2.5	17.2	134.3	20.2	134.4

Three directions are tested in experiments, including parallel to the X axis, Y shaft angle of 45° and parallel to the Y axis. The experiment results show that the vibrations of parallel to the X axis are more stable than that of the other two directions. Along the cutting direction, the curvature of workpiece changes, and the distribution of hardness influences the tool vibration greatly, but the tool vibration is centrifugal force excitation. When the tool is reaching the soft parts of the 7CrSiMnMoV, its vibration changes smoothly and the vibration amplitude is lower. When reaching the hard parts of the Cr12MoV, the tool vibration changes with fluctuations and the tool vibration amplitude increases. Experimental and simulation results are shown in Fig. 14.

High speed milling dynamics simulations at the same cutting parameters are performed and the results are shown in Fig. 15. In the process of the milling hardness splicing specimen with the high speed, spectrum value of the first frequency (134 Hz) of the milling cutter for the two kinds of materials are basically the same, and the vibration caused by the cutter error and centrifugal force are unanimous. The cutting force frequency is 268 Hz. The spectrum values of cutting 7CrSiMnMoV are lower than that of cutting Cr12MoV.

Therefore, if the cutting force is smaller, the amplitude of whole tool vibration is low and the waveform is gentle. In the machining of the Cr12MoV hardened steel specimens, the cutting force increases greatly, which is caused by the mutation of the hardness. The tool amplitude increase, but the surface roughness of cutting two materials can reach 0.8 μm, and meet the requirements of the mold surface quality.

The first order natural frequency of the cutter is 1752.5 Hz, and the resonance region is 584 Hz - 5258 Hz. When cutting and splicing specimens, tool vibration is violent in the Cr12MoV hardened steel specimens, and the spectrum of the maximum amplitude of vibration is shown in Fig. 16. The excitation frequency is the frequency of the centrifugal force, and the cutting tool error and the unbalance of the tool are the main factors to cause vibration. The value of the spectrum at the octave is less than that of the frequency spectrum. The value of the tool vibration frequency is 134 Hz, is far less than that of the resonance region. The maximum amplitude of vibration mill measured is 18.2 μm, is less than 26.8 μm which is the maximum amplitude allowed in tooth cutting.

When the spindle speed is 8000 rpm, high frequency vibration does not appear in high speed milling splice specimens. The high speed milling splice specimens is in a stable position. The stable cutting speed range should be carefully controlled from 6000 rpm to 8000 rpm.

4. Conclusion

The hardness of the material is the key character of the workpiece surface topography. In this paper the hardened steel surface hardness distribution influence on the vibration characteristics and surface morphology is analyzed by establishing an amendatory vibration model, to find the influence rule on surface morphology. Then simulations are performed based on the model, to find the stable cutting conditions. The conclusions are:

1) Cutting force and vibration model can reflect the actual cutting vibration.

2) Through the splicing hardness distribution, hardness test and high speed milling experiments, the hardness distribution's effect on the surface morphology significantly is confirmed.

3) The dynamic simulation analysis shows that the cutting conditions of stability and with these parameters the requirements of surface quality can be reached.

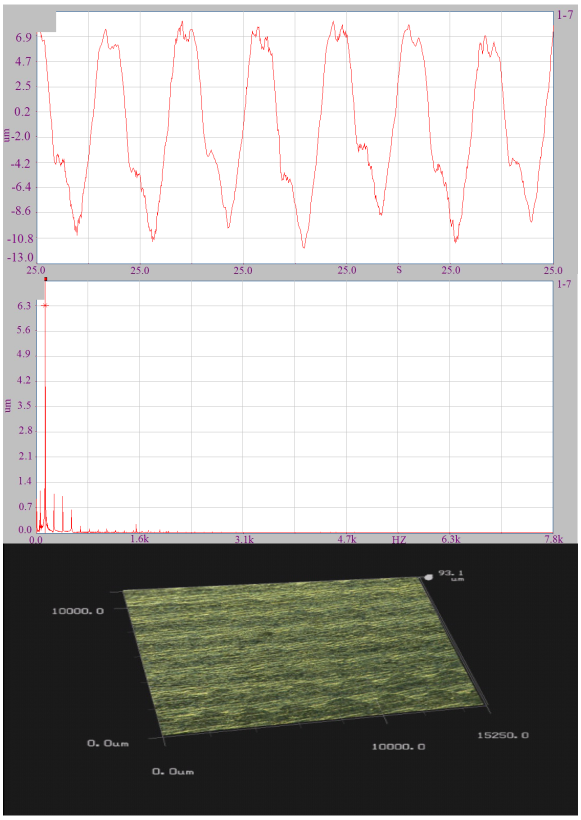

(a) The test results of cutting 7CrSiMnMoV vibration waveform, spectrum and surface micro topography.

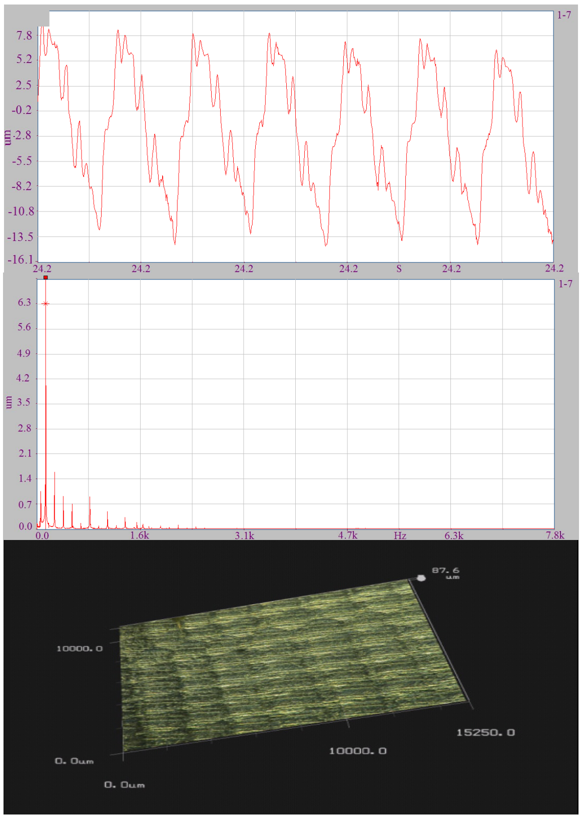

(b) The test results of cutting Cr12MoV vibration waveform, spectrum and surface micro topography.

Fig. 14. Tool vibration experiment of high-speed milling splicing workpiece.

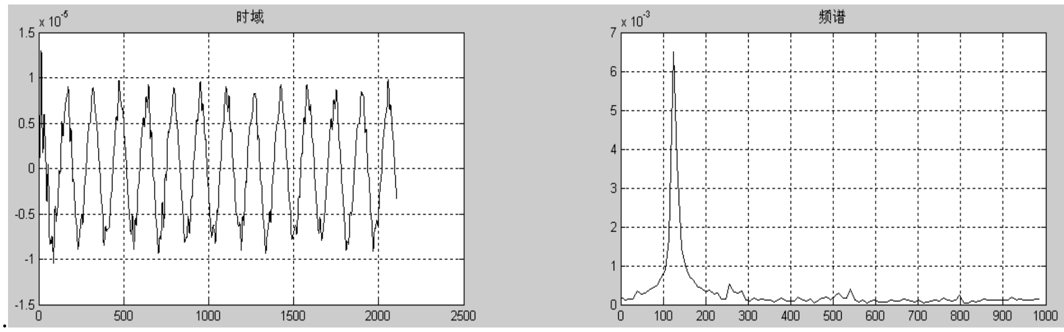

(a) 7CrSiMnMoV vibration waveform, spectrum simulation results.

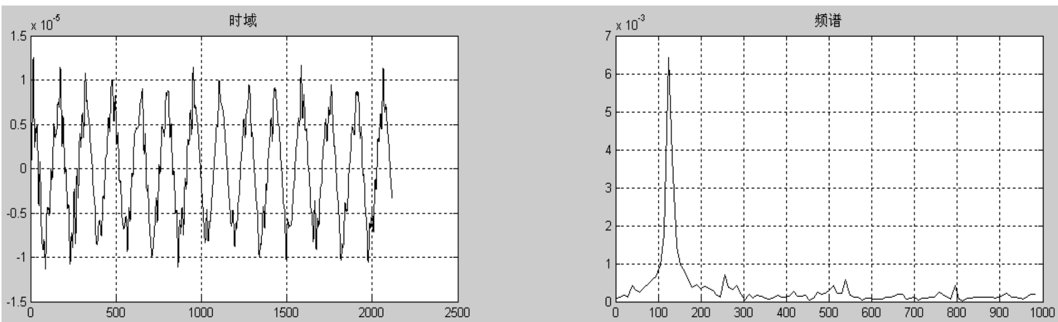

(b) Cr12MoV vibration waveform, spectrum simulation results.

Fig. 15. Tool vibration simulation of high-speed milling splicing workpiece.

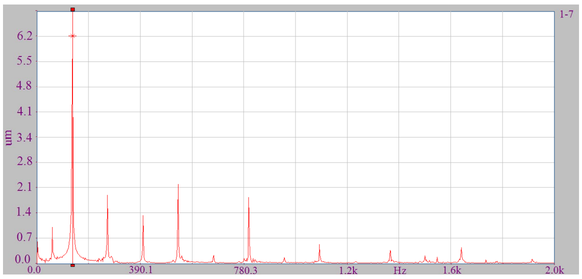

(a) feed.

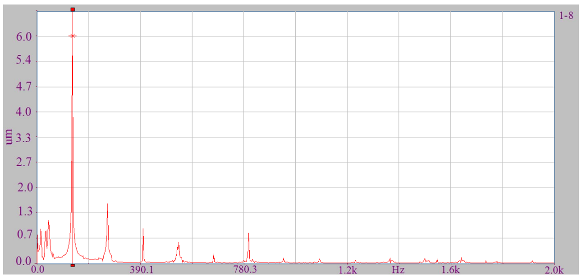

(b) row.

Fig. 16. Vibration spectrum of experimental tool.

References

[1]. C. R. Liu, M. M. Barash, The mechanical state of the sub-layer of a surface generated by chip-removal process, *Journal of Engineering for Industry*, 98, 4, 1976, pp. 1202-1208.

[2]. C. R. Liu, S. Mittal, Optimal pre-stressing the surface of a component by super-finish hard turning for maximum fatigue life in rolling contact, *Wear,* 219, 1998, pp. 128-140.

[3]. A. M. Abrao, D. K. Aspinwuall, The surface integrity of turned and ground hardened bearing steel, *Wear,* 196, 1996, pp. 279-284.

[4]. D. W. Wu, Y. Matsumoto, The effect of hardness on residual stresses in orthogonal machining of AISI 4340 steel, *Journal of Engineering for Industry*, 112, 1990, pp. 245-252.

[5]. D. A. Axinte, R. C. Dewes, Surface integrity of hot work tool after high speed milling-experimental data and empirical models, *Journal of Materials Processing Technology,* 5, 1, 2002, pp. 325-335.

[6]. X. L. Liu, The critical hardness of hard state ten in this formula: cutting, *Chinese Journal of Mechanical Engineering,* 3, 2000, pp. 9-13.

[7]. Y. Kevin Chou, Chris J. Evans, White layers and thermal modeling of hard turned surfaces, *International Journal of Machine Tools & Manufacture,* 39, 1999, pp. 1863-1881.

[8]. B. J. Griffiths, White layer formations at machined surfaces and their relationship to white layer formation at worn surfaces, *Journal of Tribology*, 107, 1995, pp. 165-171.

[9]. J. Z. Pang, M. J. Wang, C. Z. Duan, et al., Cutting force in high speed milling of hardened steel P20 and 45, *China Mechanical Engineering*, 18, 21, 2007, pp. 2543-2546.

[10]. X. L. Liu, Z. J. Yuan, The critical hardness when hard dry cutting GCr15, *Chinese Journal of Mechanical Engineering,* 36, 3, 2000, pp. 13-16.

[11]. K. Tatar, P. Gren, Measurement of milling tool vibrations during cutting using laser vibrometer, *International Journal of Machine Tools & Manufacture,* 48, 3, 2008, pp. 380-387.

[12]. A. K. Amina M., A. U. Patwari, M. S. Sharulhazrin et al., Investigation of effect of chatter amplitude on surface roughness during end milling of medium carbonsteel, in *Proceedings of the 2010 International Conference on Industrial Engineering and Operations Management,* Dhaka, University of Dhaka, 2010, pp. 131-136.

[13]. Tohck, Vibration Analyze: High Speed Rough and Finish Milling Hardened Steel, *Journal of Sound and Vibration,* 278, 1, 2004, pp. 101-115.

[14]. Z. B. Liu, X .B. Wang, Z. P. Fang, Principal composition Analyze: the characteristic parameter of vibration signal in micro-milling process, *Nanotechnology and Precision Engineering*, 8, 3, 2010, pp. 269-274.